Multiscale computational models for simulating relative permeability in complex carbonate rock sample

Guangyuan Sun[1,*], *Rafael* Salazar-Tio[1], *Jingjing* Yang[1], *Hiroshi* Otomo[1], *Ganapathi* Balasubramanian[1], *Ashraful* Islam[1], *Andrew* Fager[1], *Bernd* Crouse[1], *Raoyang* Zhang[1], *Josephina* Schembre-McCabe[2]

[1]Dassault Systèmes, USA
[2]Chevron Technical Center, a division of Chevron U.S.A. Inc,

Abstract. Relative permeability for multiphase flow through porous media is an essential petrophysical property for evaluating the hydrocarbon production in the oil and gas industry. The numerical analysis of relative permeability using digital rock is a complex problem especially for rocks exhibiting pores with multiple length scales. In digital rock analysis, micro-CT images of sufficient resolution and quality are necessary to capture the pore-scale geometry of the rock and perform direct numerical simulation of the flow. However, there is always a tradeoff between image resolution and computational cost associated to model size analysed, and a single scale image cannot resolve all pore sizes for heterogeneous rocks. In the present study, a unique multiscale extension to the multiphase Lattice Boltzmann model (LBM) is developed to study relative permeability in a typical heterogeneous carbonate rock sample. In a heterogeneous carbonate rock micro-CT image, the relatively large pores are resolvable while others are under-resolved and can be treated as an effective porous media (PM). The flow behaviour of the segmented PM regions is represented by a set of constitutive relationships (absolute permeability, k_0, capillary pressure, P_c, and relative permeability, k_r) that are precomputed on a suitable sample of PM material type. The relative permeability simulated by the multiscale model is compared with results from a high resolution model and shows good agreement to this validation data. The developed LBM extension and proposed workflow can be utilized to numerically predict relative permeability of rocks with multiple pore length scales such as carbonates, shales and tight sandstones.

1 Introduction

Multiphase flow in natural rocks is a process of significant importance in many geological study areas, such as hydrocarbon production, and storage of CO_2 and natural gas in geological reservoirs. The design and management of these applications rely on reservoir-scale models, which require petrophysical rock properties as input for accurate representation. Essential properties in this context are capillary pressure (P_c) and relative permeability (k_r) which are complex nature and time consuming to measure. In rocks with complex pore structures including multiple spatial scales, for example, carbonates and clay-rich tight sandstones, these properties can strongly deviate from classical relationships. Therefore, there is a large interest to understand the physics underlying the multiphase flow behavior of such multiscale heterogeneous samples.

Digital rock technology has been developed in the past two decades. It involves the construction of 3D representation structures at the pore-scale and offers a direct presentation of multiphase flow properties at reservoir conditions. This development was possible thanks to the availability of 3D imaging technology such as x-ray micro-tomography (micro-CT), and high performance computing, which allows to simulate oil/water flow on large complex pore structures models extracted from a micro-CT image of a rock sample. Flow simulations based on the Lattice Boltzmann method (LBM) have been particularly successful due to the level of accuracy on capturing the relevant physics of multiphase flow and wettability [1-7]. The LBM solver approximately solves the three-dimensional transient Navier-Stokes equation and provides detailed insights into the flow dynamics inside a complex rock geometry. However, rocks with pore sizes spanning multiple scales have been challenging for digital rock simulations, since micro-CT imaging focuses on a single scale and there is a tradeoff between enough resolution to capture the most relevant pore types and large enough volume to be statistically representative. Therefore, some pore types are left under-resolved in micro-CT images, and ignoring their contribution to flow simulation can lead to large errors, particularly for two-phase flow simulations where the wetting-phase connectivity in the under-resolved pores can be critical in understanding multiphase flow mechanisms.

There are several studies on multiscale extensions of multi-phase pore-network models [24, 25], and on single phase multiscale simulations with voxel based models like LBM solver where the viscous force from under-resolved porous media was modeled by a resistance term in the Brinkman equation and its permeability was derived at finer resolutions [26-32]. Recent studies [33-34] have discussed multiphase fluid flow in the multiscale pore structures. The study in [33] computed relative permeability by solving the transport equation for the total energy, Helmholtz free and kinetic energy without referring to physical properties such as the capillary

* Corresponding author: Guangyuan.SUN@3ds.com

pressure. In [34], the saturations are calculated in the finer scale using a Young-Laplace relationship and used to estimate capillary pressure in under-resolved regions, but there was no fluid simulation with pore connectivity.

In the previous study [8-11] we introduced an extension to our LBM fluid flow solver to account for single-phase and two-phase flow in under-resolved porous regions in addition to resolved pores and presented simulation results for absolute permeability and capillary pressure [10]. In this study we describe an extension of multiscale workflow to relative permeability simulations to investigate the impact of under-resolved pores on multiphase fluid flow.

2 Methodology

The multiscale workflow introduced in [8, 10] is based on a fundamental assumption of pore typing. Similar to the lithology rock typing at the sedimentary scale, we can have a classification of pore types based on similarity in pore structure topology. This assumption allows us to simplify the problem into two parts: (1) Classify a large set of regions as belonging to the same PM pore-type; (2) chose one sample of the PM pore-type regions to represent them all.

This representative PM pore-type sample can be 3D imaged at high resolution using for instance focus ion beam microscopy or laser confocal microscopy, and the resulting high resolution 3D model can be used to simulate the flow curves for this PM pore-type class.

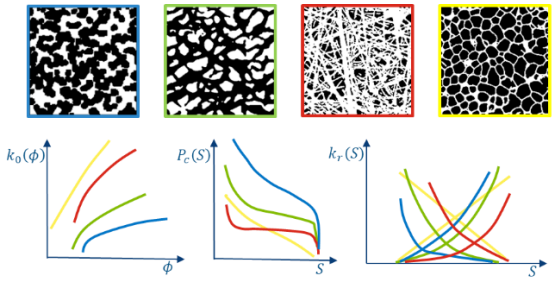

Fig. 1. Pore-type correspondence with constitutive relationships.

There is a distinctive relationship between a pore-type micro-structure and the resulting flow curves. A set of flow curves that completely represent the two-phase flow behavior of a pore-type micro-structure are: absolute permeability $k_0(\phi)$, capillary pressure $P_c(S)$, and relative permeability $k_r(S)$; together they are referred to as "constitutive relationships" in this study. In Figure 1 we show an example of four different pore-type micro-structures and the associated constitutive relationships.

This unique approach allows fluid flow in both resolved and under-resolved pore space, where pre-computed constitutive relationships are used to describe the flow in those under-resolved regions like in a continuum two-phase flow model. The under-resolved pore regions are referred to as porous media or PM regions. Although in the study cases shown in this paper we use only one PM pore-type, the workflow can work with multiple PM pore-types as far as we are able to differentiate them in the segmentation step and obtain one sample per PM pore-type to compute their corresponding constitutive relationships. In this section we will describe the general multiscale workflow, the LBM method and its extensions for multiscale scenarios. Afterwards, the specific setup for the multiscale relative permeability simulations is provided.

2.1 Multiscale workflow

The multiscale workflow introduced in [8, 10] is outlined in Figure 2 illustrating its application to a carbonate rock sample where large pores (vugs) are present along with microporous PM regions (diagenetic micrite). This workflow consists of modelling two scales, namely a large scale at coarse resolution (micro-CT segmentation and porosity estimation), and a small scale at high resolution (simulation of PM constitutive relationships). On the large scale, the micro-CT scan 3D image is analysed to classify each gray-scale voxel as pore, solid or PM, and along with an estimation of local porosity for each voxel, 1 for pore, 0 for solid, and [0-1] for PM. On the small scale, a representative model of the under-resolved PM region is used for simulation to obtain physical properties such as absolute permeability $k_0(\phi)$, capillary pressure $P_c(S)$, and relative permeability $k_r(S)$ with respect to the local porosity and the local water saturation. Finally, the results of small and large scale analyses are used as input to perform the multiscale multiphase simulation. More details of this multiscale workflow are available in [8, 10]. The present work starts from this multiscale framework, but focuses on further improvements and specific setup for relative permeability $k_r(S)$.

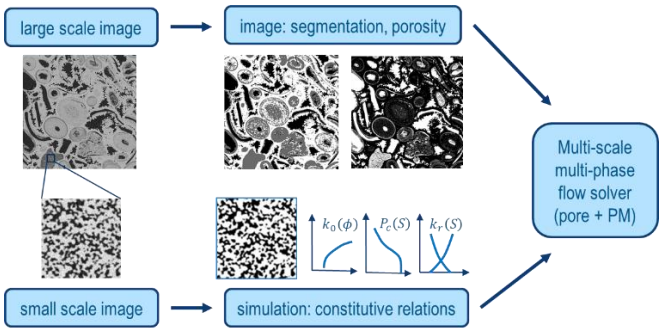

Fig. 2. Multiscale workflow. [12]

On the large scale, the micro-CT scan 3D images are analysed and segmented, which means identifying resolved pore and under-resolved pore regions. The under-resolved pore regions contain voxels where the pore structure is smaller than the micro-CT image resolution, which we label as porous media (PM) voxels. In a typical image segmentation, pore and solid voxels are shown as black and white, while a gray scale indicates a PM voxel as shown in Figure 2. Our previous study [8, 10] shows how a numerical model in terms of the solid/pore fraction accounts for the under-resolved porous structure's effects in PM voxels. It is common to have under-resolved regions with different distinct characteristics. The PM voxels are grouped according to their similar attributes, e.g. shape (channel-like or web-like), grain size or heterogeneity. Each group is assigned an ID (i.e., pore-type number) and is characterized separately. Local porosity values in under-resolved PM regions can be

estimated by a linear transformation from the micro-CT grayscale values as mentioned in the previous paragraph, and the transformation is performed on the entire PM region of a given PM pore-type. Alternatively, a porosity model can also be generated statistically with some knowledge of mean porosity and standard deviation, and the image porosity can be further improved by applying a Gaussian smoothing filter to remove the noise.

If the constitutive relationships of the under-resolved PM pore-types can be associated to existing models in a library of pre-computed PM models, the segmentation, porosity image, and the constitutive relationships for the PM pore-types will be sufficient for our multiscale multiphase flow solver to perform an accurate simulation. On the other hand, if the PM pore-types at hand are new to the library, we need to obtain a high resolution 3D image model of a representative region of the PM pore-type in order to perform fully resolved flow simulations to obtain the corresponding set of constitutive relationships which will be used to define the effective flow resistance and capillary force in the PM voxels as described in the next section.

2.2 Lattice Boltzmann method and multiscale extension

The lattice Boltzmann method (LBM) is a computational fluid dynamics (CFD) technique that has gained popularity among petroleum engineers for its suitability to simulate fluid flow in complex geometries such as in reservoir rock porous structures. It offers a unique and efficient approach to model complex multiphase flow phenomena, such as oil and gas reservoir behavior, with its ability to capture both macroscopic and mesoscopic flow properties [13-17]. LBM is well-suited to simulate complex phenomena such as multicomponent fluid interaction, fluid-solid interaction, immiscibility, and capillary effects. Due to the wide range of length scales in pore sizes present in some important reservoir rock samples, such as carbonates, typically from nanometers to millimeters, our proposed solution and workflow represent an effective technology to provide a robust and accurate multiscale simulation.

The LBM approach is based on the kinetic theory, which describes fluids as ensembles of particles, neither single particles nor continuous flows. The ensembles of particles evolve by advection, diffusion, and collision, which are governed by the Boltzmann equation. Multiple fluids types and phases can be included as components. The equation of motion for the distribution function f_i^α of the component α in the LBM is defined as,

$$f_i^\alpha(\vec{x} + \vec{c_i}\Delta t, t + \Delta t) - f_i^\alpha(\vec{x}, t) = \mathcal{C}_i^\alpha + \mathcal{F}_i^\alpha, \qquad (1)$$

where $\mathcal{C}$ is the collision operator and $\mathcal{F}$ is body force which includes gravity and intercomponent force [18-20]. Macroscopic properties, such as density and momentum, are obtained by taking the moments of f_i^α. For the intercomponent force formulation, we employ the Shan-Chen model [8,9], which is written as,

$$\vec{F}^{\alpha,\beta}(\vec{x}) = G\rho^\alpha(\vec{x}) \sum_i w_i \vec{c_i} \rho^\beta(\vec{x} + \vec{c_i}\Delta t). \qquad (2)$$

A model parameter G is calibrated so that the resulted surface tension match a target value (i.e. 30 dynes/cm for instance).

In order to extend the LBM to multiscale scenarios, we need to consider the behavior of the PM voxels in Equation 1. For a given PM voxel we can use the segmented and porosity images to assign to it a PM pore-type and a porosity value. Those values can be used in turn to assign from the corresponding constitutive relationships curves values for $k_0(\phi)$, $P_c(S)$, and $k_r(S)$, that govern the local flow field behaviour, and can be used to define an effective flow resistance and capillary force in this PM voxel as follows. A fluid flow resistance or viscous force in the under-resolved regions is modelled as the following,

$$\vec{F}_{PM\_vis}^\alpha = -\frac{\nu^\alpha}{K_0 K_r^\alpha}\rho^\alpha \vec{u}^\alpha, \qquad (3)$$

Here, $\alpha \in \{oil, water\}$ is the component index. The definition of the variables and homogeneous assumption in the underlying pore/solid structure of the PM region are discussed in [8]. K_0 is the absolute permeability, K_r^α is the α component relative permeability, ρ^α is the α component density and $\vec{u}^\alpha$ is the α component velocity. A fluid capillary force is modeled as the following,

$$\vec{F}_{PM\_cap}^\alpha = -\frac{2\sigma cos\theta J}{\sqrt{\frac{K_0 K_r^\alpha}{\phi}}}\left(\widehat{\nabla\rho^{\alpha_1}}\right) \cdot H(At, |\partial_x(At)|), \qquad (4)$$

Here, θ is the contact angle in the PM region, ϕ is porosity as a function of location, J is the Leverett J-function which is a normalized capillary force and H is a switch function that is designed to control excessive artificial forces. Here, $At = (\rho^{\alpha_1} - \rho^{\alpha_2})/(\rho^{\alpha_1} + \rho^{\alpha_2})$. Wettability models follows [8, 9, 11], where the wall potential originated from the solid part of the PM regions is constructed by a porosity-weighted average of fluid density and the prescribed wall potential.

2.3 Multiscale relative permeability simulation setup

We compute relative permeability in this work by simulating the application of a steady-state imbibition displacement method. A displacement simulation starts with an initial condition, and the simulation proceeds until the total flow rate is converged, at which point the permeability is computed. Then the oil and water mixture with increased water fraction is injected until the next water saturation level is reached. The saturation of the simulation is held constant until the flow rate is converged to achieve equilibrium. At this point the permeability of oil and water is computed again at the current saturation. The same process will be repeated until the residual condition is reached when the water phase barely moves. Periodic boundary conditions and a driving force are applied in the flow direction. Additional details for this steady state imbibition displacement method can be found in [21, 22].

The initial condition for the fluid distribution is established by a primary drainage computation. In the present study, we use the extended multiscale primary drainage method described in reference [10], based on an extended Young-Laplace relationship between capillary pressure and the local pore radius. In the original implementation for

primary drainage, a percolation invasion process is followed by increasing the pressure, a.k.a. decreasing the radius, however radiuses smaller than the pixel size cannot be archived. Therefore penetration of fluid in pores smaller than the pixel size, such as the PM under-resolved regions, cannot be simulated. In the extended Young-Laplace method described in reference [10], we introduce the definition of an effective radii smaller than a pixel size associated to the local porosity and permeability of the i PM voxel, $r_e(\phi_i) = \sqrt{k(\phi_i)/\phi_i}$, and use a similar percolation invasion process including both resolved and under-resolved pores. In this work we use this extended primary drainage method to generate the initial condition for the fluid distribution, having around 5%-10% volume corresponding to the smallest pore sizes occupied by water mostly in the PM regions and we use 30º contact angle assigned to all the surfaces for a uniform water-wet condition. All the simulations reported in this study were performed under capillary dominated displacement regime with capillary number $N_c \sim 10^{-5}$, which is given by:

$$N_c = \frac{q\mu}{\sigma} \tag{5}$$

where q is the Darcy velocity, μ is the viscosity of the invading fluid and σ is the interfacial tension between water and oil.

3 Results and discussion

3.1 Multiphase k_r imbibition of benchmark rock

The first model used for testing and benchmarking the multiscale multiphase k_r workflow is a synthetic rock sample, created by combining two scales of a porous medium: A Fontainebleau rock model with 20% of the grains replaced by a homogeneous isotropic microporous media structure, as shown in Figure 3 (top-left). We will compare two version of this synthetic model: (1) the original dual porosity model that fully resolves both pore sizes at 1 μm/voxel, 800^3 volume. We can simulate this large model with the single scale LBM solver and use the results as reference; (2) the coarsen model that only resolves the large pores at 8μm/voxel, 100^3 volume, while the small pores are under-resolved and considered as a PM pore-type. We can simulate this small model with the multiscale LBM solver.

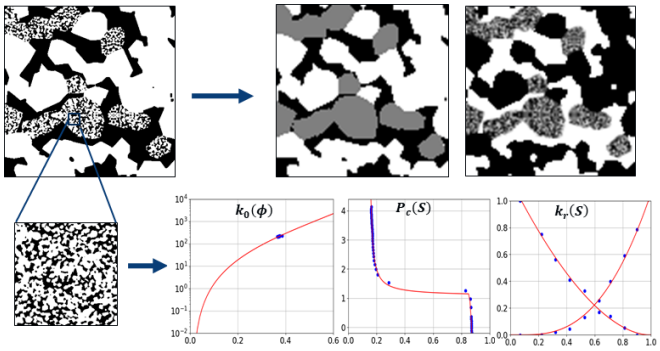

Fig. 3. Multiscale workflow from Figure 2 for the case of the Synthetic benchmark model and its multiscale inputs. The segmented image of the coarsen 100^3 model (top-middle) shows black for fluid regions, white for solid regions, and grey for PM regions and the porosity image (top-right) ranges [0:1], white is resolved pore space, grayscale is under-resolved PM region and black is solid.

In Figure 3 we show the preparation of inputs for the 100^3 model multiscale simulation, following the workflow setup from Figure 2. These inputs include: 100^3 segmentation and porosity models and the constitutive relationships (K_0, P_c and K_r) that were computed for the PM pore-type model we used to replace some of the grains. As for the advantage of the use of a smaller model, assuming that the coarse model resolution and the resolution for the fluid dynamics simulation are identical, this results in a significant reduction in the required computational volume by a factor of 8^3 in this study.

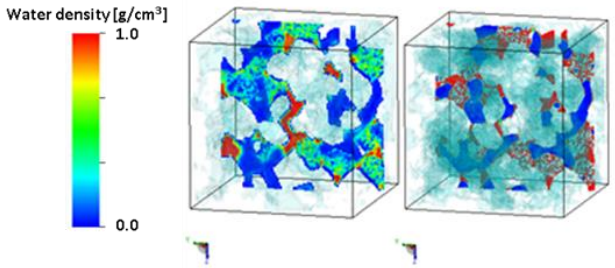

Fig. 4. 3D view of water distribution (transparent light blue) coupled with a slice view of water density for multiscale 100^3 model (left) and single resolution 800^3 model (right) at water saturation = 40%.

The total pore space is 29.3% for 800^3 fully resolved model and 28.5% for 100^3 coarsen model, which includes porosity contributions from both resolved and under-resolved pore regions. A steady-state imbibition K_r simulation is performed for each case with our optimized water injection method [8, 10]. In Figure 4, a comparison of results for fluid distributions shows the consistency between the fully resolved simulation and the multiscale simulation, as shown by a comparable invasion pattern achieved.

Next we look at the simulation results for relative permeability. Figure 5 shows the comparison of relative permeability between the single-scale fully resolved model and the multiscale model. It indicates that, even though there is 8^3 times difference in resolution, both models show overall good agreement. The cross-over point where water/oil permeabilities are equal and the amount of residual oil are corresponding [23].

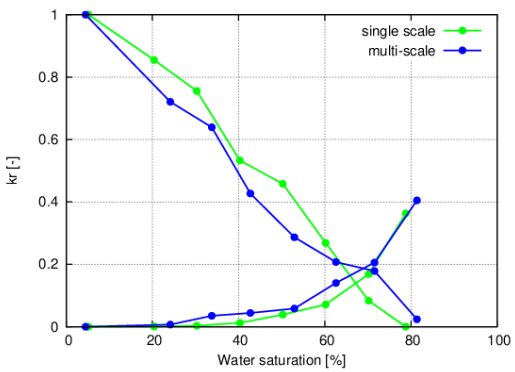

Fig. 5. Water and oil relative permeability curves comparison between 100^3 volume (blue) and 800^3 volume (red).

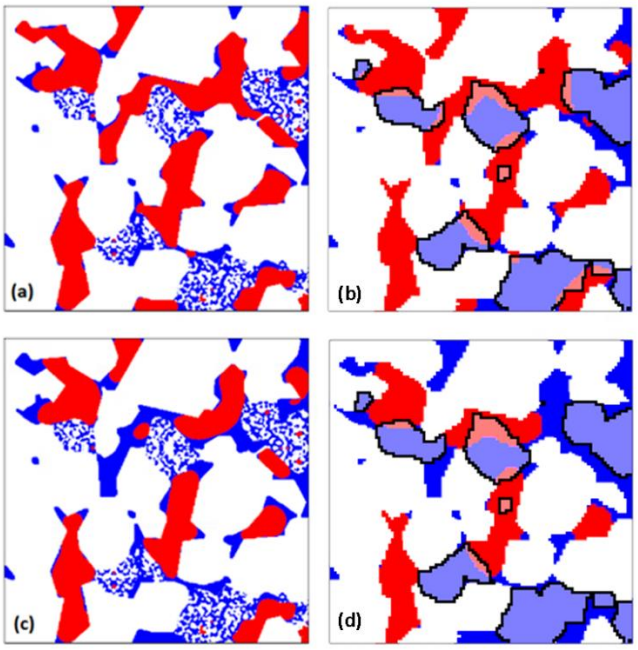

Fig. 6. Fluid distribution (red: oil; blue: water) in the fully resolved single resolution model (left column) and multiscale model (right column) and at water saturation = 40% (a, b) and = 60% (c, d). PM regions in multiscale model (right) are shown by regions within the black contours where light blue and light red colors indicate water and oil in the PM region, respectively.

In Figure 6, the water distribution is compared at two stages where water saturation is at 40% and 60%. Blue and red represent the two phases, water and oil. Water first invades small pores, most of which are in the under-resolved regions (Figure 6(a) and 6(b)) at Sw=40%, then expands its front toward resolved pore space at Sw=60% (Figure 6(c) and 6(d)). Throughout the imbibition process, the flow patterns show a close match between the two models.

The above test case serves as a validation of the multiscale LBM kr workflow. In the next section we apply this workflow to a realistic rock sample case, where sample images are captured at two different resolution using different microscopy imaging techniques.

3.2 Carbonate sample and previous multiscale results

In Figure 7 we show the Indiana Limestone rock sample used in this study [10] and the preparation of inputs for the multiscale multiphase LBM flow solver, as described in the workflow setup from Figure 2. These inputs include: segmentation and porosity image and constitutive relationships for the segmented PM pore-type regions.

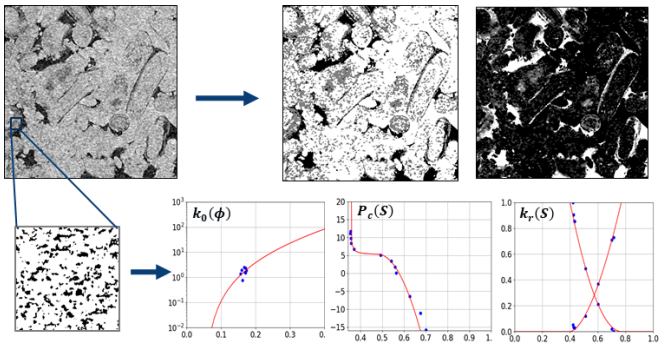

Fig. 7. Multiscale workflow from Figure 2 for the case of the Indiana Limestone sample and its multiscale inputs

Experimental values for porosity and permeability of this rock sample are around 16% and 7 mD, respectively. Mercury porosimetry shows two pore-type peaks around 5 μm and 0.4 μm pore-throat radius. The micro-CT images were acquired at 3.5 μm/pixel and a volume of 600^3 was extracted. At this resolution, only the large pore-type is resolved. The smaller pore-type correspond to a diagenetic micrite mineral and constitutes the under-resolved PM pore-type for this multiscale simulation. As described in [10] a high resolution PM model was obtained using laser confocal scanning microscopy at 0.128 μm/pixel, sufficient resolution to capture this smaller pore-type. The results for porosity and permeability for this micrite 3D model are 18.2% and 1.7 mD, and the constitutive relationships were also computed and shown in Figure 7. The $k_0(\phi)$ curve is fitted from eight subdomain simulations from the micrite 3D model. The dependence of $P_c(S)$ and $k_r(S)$ on saturation is fitted from results of two-phase simulations with assumed wetting conditions, initial saturation and a surface tension of 30 dynes/cm. More details on this Indiana Limestone rock sample, micro-CT and confocal models as well as constitutive relationship calculations can be found in our previous study [10].

In Figure 8 we show results from single-phase flow LBM simulation in a sub-volume of the original microCT model comparing the velocities on the single-scale case to the multiscale case. It is clear from this comparison that adding PM regions in the simulation opens new paths for flow, however due to the large permeability difference between resolved pores and under-resolved pores, the majority of the flow goes preferentially to the larger pores (resolved). This is reflected on the overall similar permeability simulation results.

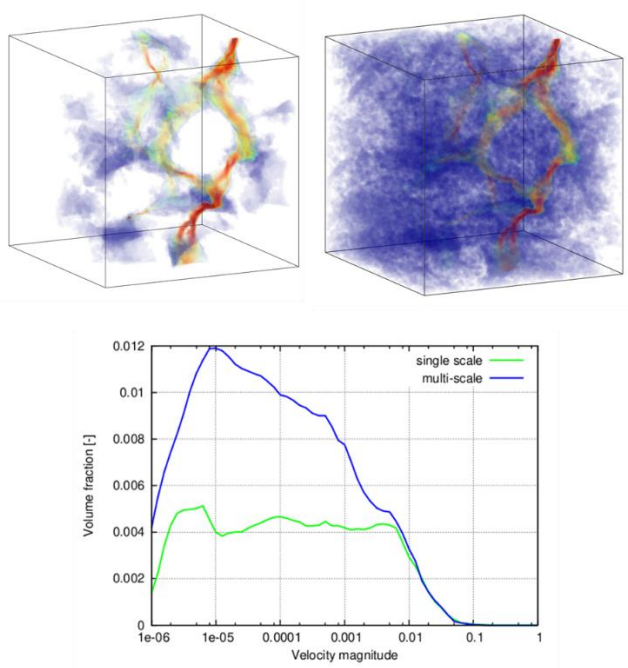

Fig. 8. Flow velocity 3D field and distribution function of velocity magnitude. Top left: single-scale results (PM as solid); top right: multiscale results; bottom: velocity magnitude comparison.

Although the additional PM connectivity did not seem to impact the single-phase flow case significantly [10], it affects multiphase analysis including capillary pressure and relative permeability. Our previous study [10] demonstrates that for the two-phase flow capillary pressure imbibition simulation, water can more efficiently displace oil through the connectivity established by the PM region, resulting in an overall smaller values for the irreducible oil saturation, which is also consistent with the experimental observations. More details on this can be found in our previous study [10].

3.3 Multiphase k_r imbibition of carbonate rock

In this section the application of the multiscale multiphase relative permeability workflow on Indiana Limestone is presented. As a comparison to the multiscale case, we create two reference cases (1) a single resolution model with PM as solid phase, and (2) a registered high resolution confocal model which is constructed by scaling up the micro-CT model by a factor of 5, and replacing PM regions by copies of the high resolution PM pore-type 3D model shown in Figure 7 (bottom-left), and ensuring the connectivity of PM regions by periodic mirroring boundary condition.

A full size multiphase simulation of the registered model is not possible, which could result in a tremendously expensive simulation. Therefore, a heterogeneous but relatively well connected 100^3 subvolume with the resolution of 3.5 µm/pixel is chosen to validate the methodology. In this subvolume, resolved porosity is 15.44% and effective porosity from under-resolved PM is 6.83%.

Figure 9 shows the comparison of relative permeability of three models. To make the comparison consistent, the measurement of water saturation in the single resolution model with PM as solid is corrected by the ratio of resolved porosity to total porosity. It is clear that more oil is mobilized as higher effective porosity is provided. When PM is considered as solid, water only invades into resolved larger pores and thus leads to significant drop of oil permeability at low water saturation. In both, the multiscale model and registered model, the PM regions are considered as semi-permeable and able to provide additional effective connected porosity for the flow (Figure 10).

The comparison of different models is a good exercise to check the consistency between the single-scale solver and the multiscale solver. In Figure 11, the relative permeability measured by the multiscale solver shows certain similarity to the registered high resolution model measured by the single-scale solver. It is noteworthy that the way we construct the registered high resolution model is not unique, therefore the results shown on Figure 11 (left) represent only one possible realization, and the differences observed respect to the multiscale model results (right) are mainly due to this non-uniqueness, nevertheless it still provides a representative outcome for qualitative comparison.

This kind of comparison can also provide the boundary of relative permeabilities for different treatments of under-resolved regions. The contribution of under-resolved PM regions to the overall flow is not negligible. As PM regions becomes less permeable, the flow behaviour is observed to be similar to the one exhibited by the single resolution case with PM as solid.

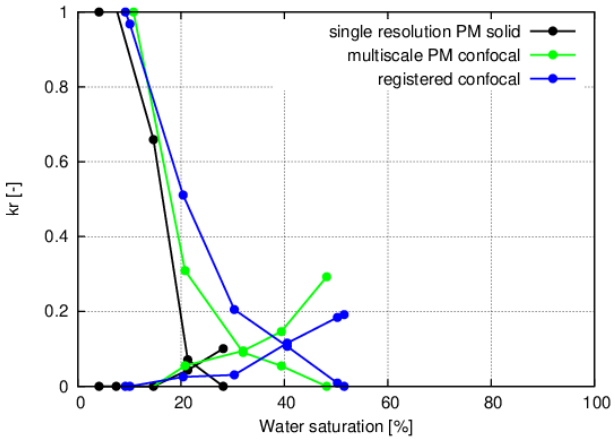

Fig. 9. Comparison of relative permeability curves for the 100^3 cases.

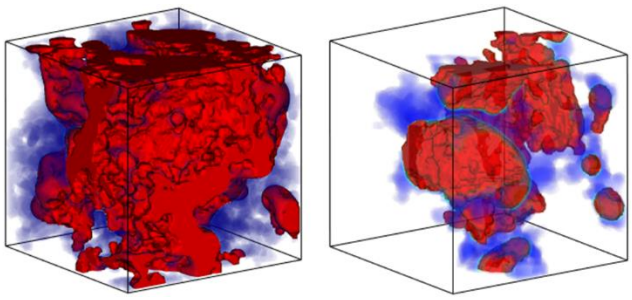

Fig. 10. 3D view of the distribution of water (blue) and oil (red) in the multiscale model (left) and single resolution model with PM as solid (right) at water saturation = 20%.

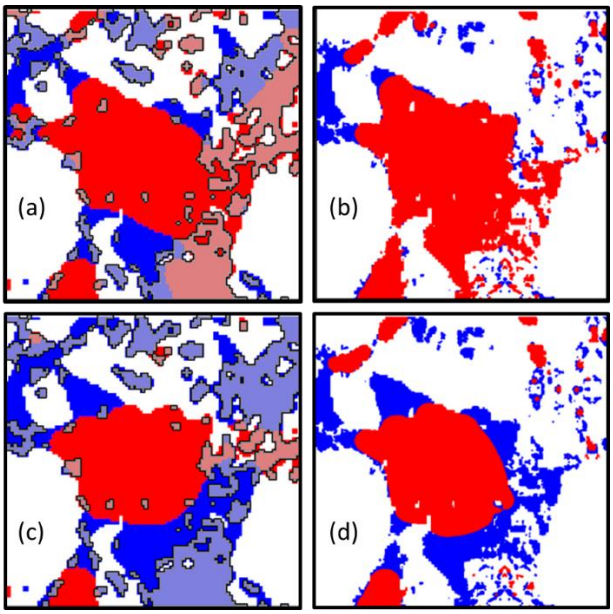

Fig. 11. Fluid distribution (red: oil; blue: water) in the multiscale model (left column) and registered high resolution model (right column) at water saturation = 20% (a, b) and = 50% (c, d). PM regions in multiscale model (left) are shown by regions within the black contours where light blue and light red colors indicate water and oil in the PM region, respectively.

Next, we present a multiscale multiphase simulation in a larger sub-volume 500^3 with resolution of 1.75 μm/pixel. Its resolvable porosity is 6.75% and the effective porosity from under-resolved PM is 4.07%, as shown in Figure 12. The relative permeability of the PM-solid single scale (black) and PM-identified multiscale models (green) are shown in Figure 13. The oil permeability in the multiscale model is higher as more oil is mobilized due to the additional PM connectivity. The distributions of water (blue) and oil (red) corresponding to selected saturation levels as obtained in multiscale model during the steady-state relative permeability simulation are shown in Figure 14. Figure 15 shows the comparison of fluid distributions of oil and water at the same water saturation (= 30%) in the two models. Water in the multiscale model is mainly found in the two forms: (1) as a continuous film over the surface of resolved pores and (2) filling into the PM - under-resolved pores. In the single resolution model with PM as solid-, most of the water tends to move into resolved pores where oil is easily displaced.

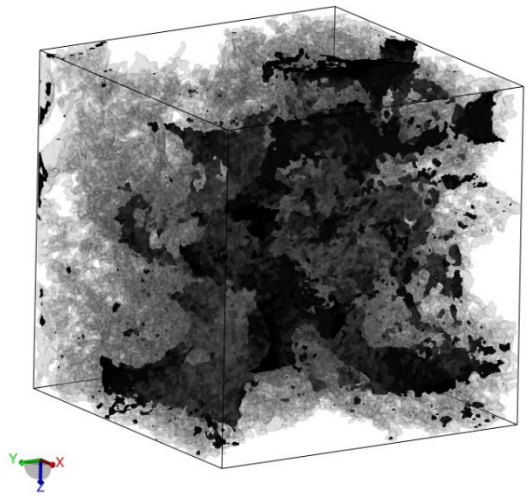

Fig. 12. 3D view of the distribution of resolved pores (black) and under-resolved PM (gray) in multiscale 500^3 model.

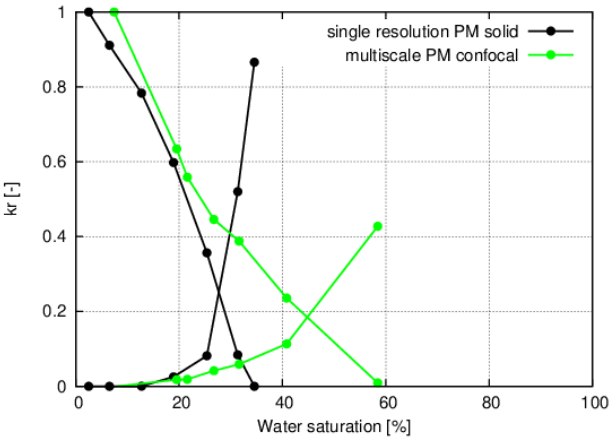

Fig. 13. Comparison of relative permeability curves for the 500^3 cases.

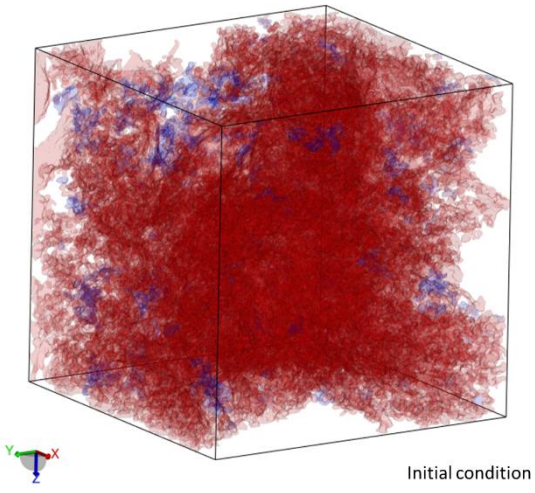

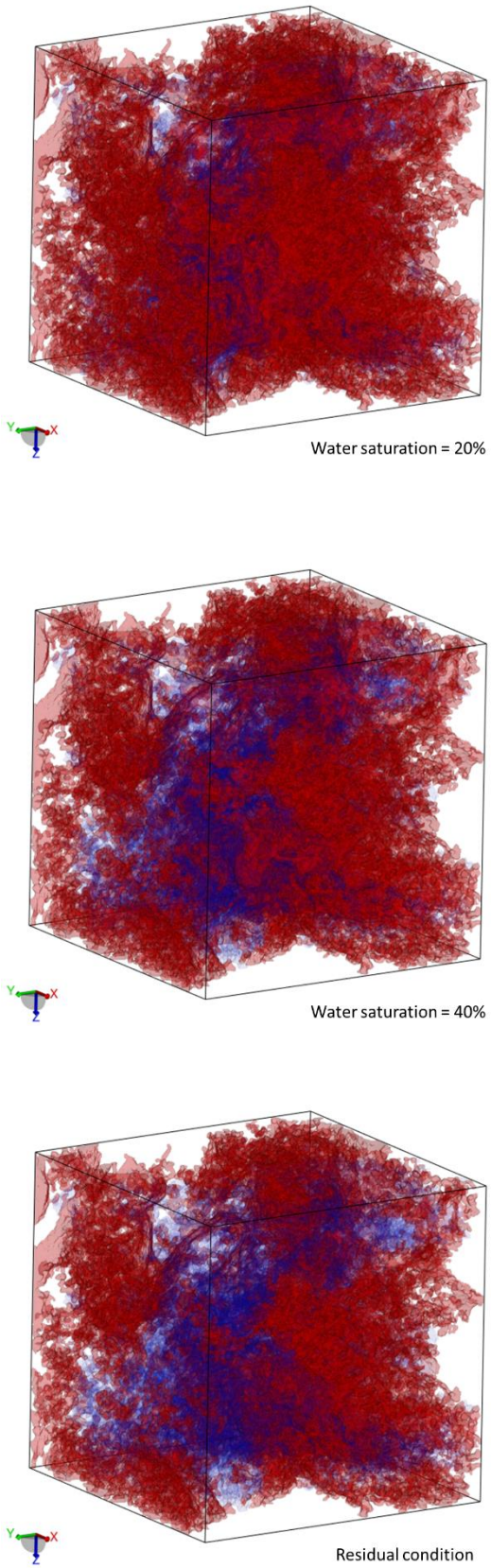

Fig. 14. 3D view of the distribution of water (blue) and oil (red) in multiscale 500^3 model at selected saturation levels.

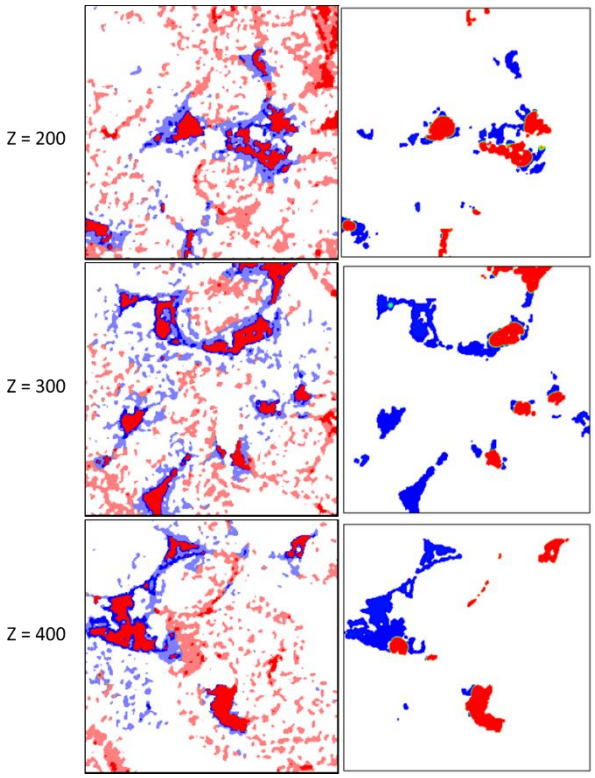

Fig. 15. Fluid distribution (red: oil; blue: water) at water saturation = 30% along different depth in flow direction (Z) (left: multiscale; right: single resolution with PM as solid). PM regions in multiscale model (left) are shown by regions within the black contours where light blue and light red colors indicate water and oil in the PM region, respectively.

4 Conclusions

We developed a new digital rock workflow applicable for multiphase relative permeability simulations on multiscale models representing complex heterogeneous rock samples, such as carbonate or clay-rich tight sandstone. In the new multiscale extension to the LBM multiphase solver, we introduce a complete workflow to identify and characterize the PM under-resolved regions by constitutive relationships. With the introduction of the fluid flow simulation into the under-resolved pores, the voxel-based LBM solver is not limited to the minimal pixel size. To validate the new workflow, we compared our simulation results of steady-state water/oil relative permeability between single resolution models (high resolution) and multiscale models (low resolution) of the same region for a synthetic sample and a heterogeneous carbonate sample. As reference cases, a single resolution model with PM regions as solid is also explored within the carbonate sample to compare with the multiscale model. It is observed that oil permeability is higher as more oil is mobilized due to high effective porosity in the multiscale model. Therefore, under-resolved pores are very important in multiscale multiphase flow in the context of oil production. This workflow not only improves the accuracy of digital rock multiphase measurement in the context of complex multiscale rock samples such as carbonates and clay-rich tight sandstones but also enables an effective

upscaling procedure to perform multiphase flow measurement on coarse resolution models.

Reference

1. X. Shan, H. Chen, Physical Review E, **47(3)**, 181 (1993).
2. B. Crouse, D. M. Freed, N. et al. SCA **2016-058** presented at the International Symposium of the Society of Core Analysts held in Snow Mass, Colorado, USA (2016)
3. G.R. Jerauld, J. Fredrich, N. Lane, Q. Sheng, B. Crouse, D. M Freed, R. Xu, In SPE Abu Dhabi International Petroleum Exhibition & Conference. Society of Petroleum Engineers. November (2017)
4. H. Otomo, H. Fan, Y. Li, M. Dressler, I. Staroselsky, R. Zhang, H. Chen, Journal of Computational Science, **17**, 334-339 (2016)
5. H. Chen, C. Teixeira, K. Molvig, International Journal of Modern Physics C, **9(08)**, 1281-1292 (1998)
6. X. Shan, X.F. Yuan, H. Chen, Journal of Fluid Mechanics, **550**, 413-441 (2006)
7. H. Otomo, B. Crouse, M. Dressler, D. M. Freed, I. Staroselsky, R. Zhang, Chen, H, Computers & Fluids, **172**, 674-682 (2018)
8. H. Otomo, R. Salazar-Tio, J. Yang, H. Fan, A. Fager, B. Crouse, R. Zhang, H. Chen, *Comm. in Comp. Phy.* **33.1** 189-213 (2023): 189-213.
9. H. Otomo, R. Salazar-Tio, H. Chen, R. Zhang, A. Fager, G. R. Balasubramanian, B. Crouse, H. Fan and J. Yang, **US Patent No. 17136259**, (2020)
10. A. Fager, H. Otomo, R. Salazar-Tio, G. Balasubramanian, B. Crouse, R. Zhang, H. Chen and J. Schembre-McCabe, The 2021 International Symposium of the Society of Core Analysts (2021): Volume 366
11. H. Otomo, B. Crouse, M. Dressler, D.M. Freed, I. Staroselsky, R. Zhang, H. Chen, Comput. & Fluids **172** 674 (2018)
12. Tom Bultreys. Savonnières carbonate. Digital Rocks Portal (September 2016)
13. Q. Li, K. H. Luo and X. J. Li, *Physical Review E* **86.1**, 016709 (2012)
14. R. Zhang, X. Shan and H. Chen, *Physical Review E* **74.4**, 046703 (2006)
15. H. Chen, C. Teixeira and K. Molving, Int. J. Mod. Phys. C, **8 C 8.04**, 675-684. (1997)
16. H. Chen, R. Zhang and P. Gopalakrishnan, US Patent No. 9,576,087, (2017)
17. H. Chen, R. Zhang and P. Gopalakrishnan, Phys. Scr., **95(3)**, 034003 (2020)
18. H. Chen, R. Zhang, I. Staroselsky and M. Jhon, Physica A, **362(1)**, 125-131. (2006)
19. X. Shan, X. Yuan and H. Chen, J. Fluid. Mech., **550**, 413-441 (2006)
20. Y. Qian, D. d'Humières and P. Lallemand, Europhys. Lett., 17(6), 479. (1992)
21. A. Fager, G. Sun, R. Xu, et al. Journal of Petroleum Science and Engineering, **208**, 109435 (2022)
22. G.R. Jerauld, J. Fredrich, N. Lane, Q. Sheng, B. Crouse, D. M Freed, R. Xu, In SPE Abu Dhabi International Petroleum Exhibition & Conference. Society of Petroleum Engineers. November (2017)
23. W. Anderson, J. Petro. Tech. **39(11)**, 1453-1468. (1987)
24. S. K. Masalmeh, X. Jing, S. Roth, C. Wang, H. Dong, M. Blunt, Society of Petroleum engineers SPE-177572-MS (2015)
25. L. C. Ruspini, G. Lindkvist, S. Bakke, L. Alberts, A. M. Carnerup, and P. E. Øren, Society of Petroleum Engineers SPE-180268-MS (2016)
26. D.M. Freed, International Journal of Modern Physics C **09**, 1491 (1998)
27. N.S. Martys, J.G. Hagedorn, Materials and Structures **35**, 650 (2002)
28. I. Ginzburg, G. Silva, L. Talon, Phys Rev E **91**, 023307 (2015)
29. J. Li, D. Brown, Geofluids, 1740693 (2017)
30. J. Zhu, J. Ma, Scientific Reports **8** 5826 (2018)
31. A. Fager, R. Salazar-Tio, G. Balasubramanian, and B. Crouse, RMAG/DWLS FALL SYMPOSIUM. Denver (2019)
32. M. Zhang, R. Salazar-Tio, A. Fager, B. Crouse, Unconventional Resources Technology Conference URTeC (2020)
33. A. Demianov, O. Dinariev, N. Evseev, The Canadian journal of chemical engineering **89,** 206 (2011)
34. M. Suhrer, X. Nie, J. Toelke, Proceedings of international petroleum technology conference, 20035 (2020)